



Controlled O₂ reduction at a mixed-valent (II,I) Cu₂S core†

Cite this: *Chem. Commun.*, 2020, 56, 9636

Received 7th June 2020,
Accepted 16th July 2020

DOI: 10.1039/d0cc03987j

rsc.li/chemcomm

Jordan Mangué,^a Clément Gondre,^a Jacques Pécaut,^b Carole Duboc,^c Stéphane Ménage^{id}^a and Stéphane Torelli^{id}*^a

Inspection of Oxygen Reduction Reactions (ORRs) using a mixed-valent Cu₂S complex as a pre-catalyst revealed a tuneable H₂O₂ vs. H₂O production under mild conditions by controlling the amount of sacrificial reducer. The fully reduced bisCu^I state is the main active species in solution, with fast kinetics. This new catalytic system is robust for H₂O₂ production with several cycles achieved and opens up perspectives for integration into devices.

With the increase in the world population and the shrinkage of unsustainable fossil fuels that we depend on, there is a crucial need to explore carbon-free alternatives to ensure a safe and sustainable future. In line with this, the so-called Oxygen Reduction Reactions (ORRs) are important processes in fuel cell technology¹ for achieving a hydrogen-based society.² However, this cathodic event remains the limiting step regarding the efficiency of a complete device.³ ORRs find their essence in Nature with biological respiration⁴ including laccases that catalyse the 4e⁻/4H⁺ reduction of O₂ to H₂O.⁵ The other important product formed upon O₂ reduction is hydrogen peroxide (H₂O₂) via a 2e⁻/2H⁺ process. H₂O₂ is important for living organisms where it is, for instance, biosynthesized by the immune system to kill microbes,⁶ a signal molecule under oxidative stress conditions⁷ or used for metabolic purposes by copper metalloenzymes such as galactose oxidase.^{5b} It is a staple in the industry with a ranking in the top 100 most important reactants with more than 3 million tons produced per year⁸ and is widely used in pharmaceuticals, cosmetics and electronics.⁹ H₂O₂ has recently emerged as a potent

latent energy carrier through its O–O bond (Gibbs free energy of formation of ΔG_f⁰ = –120 kJ mol⁻¹ from H₂ and O₂) and is thus a suitable candidate for energy storage for fuel cell technology.¹⁰ However, given that its production mainly relies on the energy-consuming and precarious anthraquinone process,¹¹ new eco-friendly methodologies for controlled H₂O₂ production from O₂ reduction are yet to be discovered.

The conception of efficient catalysts for homogeneous ORRs based on noble and also non-noble metal ions such as Fe, Co or Mn has stimulated intensive research.¹² In these cases, the electron source for the catalytic activity comes from sacrificial reducers such as metallocenes or *via* electrocatalysis. With respect to homogenous Cu-based catalysts, mono-,¹³ di-¹⁴ and trinuclear¹⁵ copper complexes have been studied and relevant activities reported. Interestingly, the presence of a Lewis acid (Sc³⁺) was shown to induce selective catalysis for two-electron O₂ reduction.¹⁶ Under heterogeneous conditions, immobilized Cu complexes are particularly efficient for O₂ reduction into H₂O.¹⁷

With the aim of targeting ORRs with original di-copper systems, we report here the activity of our previously described mixed-valent (MV) copper complex **1**¹⁸ possessing a N₆Cu₂S environment (Fig. 1). We evidenced a tuneable chemical H₂O₂ vs. H₂O selectivity in acetonitrile using controlled amounts of ferrocene derivatives as electron sources and in the presence of an organic acid. This study represents, to the best of our knowledge, the first example of a selective ORR involving a Cu₂S core under homogeneous and mild conditions.

Catalytic ORRs by **1** (0.05 mM, final concentration) were evaluated at room temperature (298 K) in air-saturated

^a Univ. Grenoble Alpes, CNRS, CEA, IRIG, Laboratoire de Chimie et Biologie des Métaux, 17 rue des Martyrs, 38054 Grenoble Cedex 9, France.
E-mail: stephane.torelli@cea.fr

^b Univ. Grenoble Alpes, CEA, CNRS, IRIG, SYMMES, UMR 5819 Equipe Chimie Interface Biologie pour l'Environnement, la Santé et la Toxicologie, 38054 Grenoble Cedex 9, France

^c Univ. Grenoble Alpes, Département de Chimie Moléculaire, 301 rue de la chimie, 38054 Grenoble Cedex 9, France

† Electronic supplementary information (ESI) available. CCDC 2014256. For ESI and crystallographic data in CIF or other electronic format see DOI: 10.1039/d0cc03987j



Fig. 1 Chemical structure of **1** and targeted ORRs.

MeCN solutions. 2,6-Lutidinium tetrafluoroborate (LutHBF₄, 400 molar equiv.) was used as an innocent proton donor (weak coordinating ability of both the conjugate base and the BF₄⁻ counter-anion) and sacrificial electrons (10 to 100 molar equiv.) were provided by means of ferrocene (Fc, $E_{1/2}$ Fc⁺⁰ = 0 V vs. Fc⁺⁰), dimethylferrocene (Me₂Fc, $E_{1/2}$ Me₂Fc⁺⁰ = -0.10 V vs. Fc⁺⁰), octamethylferrocene (Me₈Fc, $E_{1/2}$ Me₈Fc⁺⁰ = -0.42 V vs. Fc⁺⁰) or dexamethylferrocene (Me₁₀Fc, $E_{1/2}$ Me₁₀Fc⁺⁰ = -0.49 V vs. Fc⁺⁰). Fc and Me₂Fc were not compatible with the *in situ* reduction of any redox form of **1** ($E_{1/2}^1 = -0.44$ V vs. Fc⁺⁰, $\Delta E = 0.07$ V, Cu₂^{I,II} → Cu₂^I; $E_{1/2}^2 = -0.30$ V vs. Fc⁺⁰, $\Delta E = 0.08$ V, Cu₂^{I,II} → Cu₂^{II,II}),¹⁸ whereas Me₈Fc and Me₁₀Fc were suitable for these processes. Monitoring the reaction by UV-Visible (UV-vis) spectrophotometry unambiguously showed the formation of Fc⁺, Me₂Fc⁺, Me₈Fc⁺ or Me₁₀Fc⁺ at 614 nm ($\epsilon = 410$ M⁻¹ cm⁻¹), 650 nm ($\epsilon = 290$ M⁻¹ cm⁻¹), 750 nm ($\epsilon = 390$ M⁻¹ cm⁻¹) and 778 nm ($\epsilon = 495$ M⁻¹ cm⁻¹), respectively (Fig. S1–S8 and Table S1, ESI[†]) and attested to the O₂ reduction in all cases. Interestingly, only 2 molar eq. of Fc⁺ and 30 molar eq. of Me₂Fc⁺ (Fig. S3 and S4, ESI[†]) were detected when going up to 100 molar eq., whereas the maximum possible turnover numbers (TONs) are reached with Me₈Fc and Me₁₀Fc (denoted as Me_{8–10}Fc when compared in the following) regardless of the excess (Fig. 2 and Fig. S5–S8, ESI[†]).

Quantitative Me_{8–10}Fc⁺ formation allowed the use of the H₂O₂-specific TiO-type procedure (Fig. S9, ESI[†]) in order to discriminate between H₂O₂ and H₂O production.¹⁹ This method is extremely precise compared to iodine titration. H₂O production was calculated considering the amount of Me_{8–10}Fc⁺ not involved in the H₂O₂ formation (see the ESI[†] for more details).

A key result is the change in selectivity, H₂O₂ vs. H₂O, observed by varying the amount of Me_{8–10}Fc (Table 1): almost exclusive H₂O₂ formation occurs with 10 molar eq., whereas going to 100 molar eq. mainly leads to H₂O production (entries 1 and 6, Table 1). The selectivity is moderately affected by either the kinetics or the difference in the reducing abilities of Me_{8–10}Fc ($\Delta E_{1/2} = 0.07$ V). As control experiments, no O₂ or H₂O₂ reduction by Me_{8–10}Fc occurs under the same conditions

(and reaction times) in the absence of **1** (Fig. S10, ESI[†]). This strongly supports the H₂O formation process originating from a catalysed two-electron reduction of a coordinated (hydro)peroxide at high Me_{8–10}Fc concentrations. The inactivity of low-valent [Cu(Tol)₂](OTf) (OTf = trifluoromethanesulfonate anion and Tol = toluene) finally reinforces the remarkable effect of the S/N coordination spheres in **1** on the reactivity and excludes solvated Cu^I ions as activators.

Kinetically speaking, the fact that the reactions with Fc and Me₂Fc are relatively slow and not complete compared to those with Me_{8–10}Fc (Table 1 and Table S2, ESI[†]) suggests that **1** or its protonated form **1**^H (see below for the behaviour of **1** with LutHBF₄) could initiate the reaction. However, its rather modest efficiency indicates that MV states cannot be considered as the most active forms. This also demonstrates that the redox potentials of the oxidized species generated along the reaction course are not (or partially) thermodynamically compatible with the reducing abilities of Fc and Me₂Fc to reach the total consumption of the electron source.

Consequently, from now on, only the case of Me_{8–10}Fc is discussed since quantitative and fast conversions were obtained. For 10 and 20 molar eq., the kinetic traces (Fig. S5 and S7, ESI[†]) display pseudo-first-order profiles and comparable reaction times. Starting with 40 molar eq. and above, the reaction times are significantly shorter with Me₁₀Fc compared to Me₈Fc, for which successive steps are identifiable (Fig. S5–S8, ESI[†]). The overall comparison of the kinetics traces clearly indicates the involvement of more active species when using Me₁₀Fc compared to Me₈Fc. It is worth noting that the k_{obs} values are inversely proportional or quasi-independent with respect to [Me₈Fc] (to a certain extent) or [Me₁₀Fc], respectively (Fig. S11, ESI[†]). This suggests that the gradual accumulation of H₂O results in competitive reaction pathways for Me₈Fc (with a global steady state starting from 60 molar eq.) that are not present for Me₁₀Fc (its consumption not being the rate-determining step).

This new catalytic system has proven to be robust for H₂O₂ production, especially under the most favourable conditions. For instance, at least four consecutive cycles were achieved with successive addition of 10 molar eq. Me₈Fc and its quantitative consumption after each injection (Fig. S12, ESI[†]). An overall selectivity of 85% in H₂O₂, similar to that observed for a single run, was determined. This result demonstrates that H₂O₂ accumulation neither (i) affects the selectivity/efficiency nor (ii) poisons the catalyst.

The behaviour of **1** in the presence of Me_{8–10}Fc and LutHBF₄ prior to exposure to air was then investigated in order to gain insights into the nature of the putative relevant copper species involved during the O₂ reduction process. For solubility reasons, as the concentrations required to perform such experiments are different from those used for catalysis, only one condition (*i.e.* 10 molar eq. Me_{8–10}Fc and 400 molar eq. LutBF₄) was tested. Since identical results were obtained whatever the nature of the electron source, only the data obtained with Me₈Fc are discussed. Under strict anaerobic conditions, the UV-vis/NIR spectrum of **1** is modified upon addition of LutHBF₄ and/or Me₈Fc (Fig. S13, ESI[†]). The presence of protons leads to the formation of a new **1**^H species



Fig. 2 Representative UV-vis spectra for Me₈Fc⁺ accumulation during ORRs mediated by **1** in air-saturated MeCN at 298 K using **1**/Me₈Fc/LutHBF₄ at 1/20/400; inset: variation of the Abs^{750nm} as a function of time (the green dotted line indicates the theoretical A_{max} for the total Me₈Fc conversion); the black arrow indicates the injection of **1**.

Table 1 ORR experiments performed with **1** at room temperature using Me₈₋₁₀Fc and LutHBF₄ as electron and proton sources^a

Entry	[Me ₈₋₁₀ Fc] (mM)	Cat/e ⁻ /H ⁺	% H ₂ O ₂ Me ₈ Fc/ Me ₁₀ Fc	% H ₂ O Me ₈ Fc/ Me ₁₀ Fc	TON	TON _{max}	k _{obs} (s ⁻¹) Me ₈ Fc/Me ₁₀ Fc	t (s) Me ₈ Fc/Me ₁₀ Fc
1	0.5	1/10/400	90/82	10/18	10	10	1.06 ± 0.02/0.47 ± 0.02	4.1 ± 0.2/5.6 ± 0.3
2	1.0	1/20/400	83/72	17/28	20	20	0.61 ± 0.02/0.39 ± 0.02	6.5 ± 0.3/5.9 ± 0.3
3	2.0	1/40/400	57/58	43/42	40	40	0.28 ± 0.04/0.52 ± 0.03	15.0 ± 0.4/6.0 ± 0.5
4	3.0	1/60/400	51/37	49/63	60	60	0.13 ± 0.01/0.62 ± 0.04	28.1 ± 0.5/5.9 ± 0.3
5	4.0	1/80/400	38/10	62/90	80	80	0.15 ± 0.01/0.60 ± 0.03	32.1 ± 1/6.2 ± 0.3
6	5.0	1/100/400	10/5	90/95	100	100	0.12 ± 0.01/0.41 ± 0.02	41.2 ± 2/10.6 ± 0.4

^a See the ESI for further experimental details.

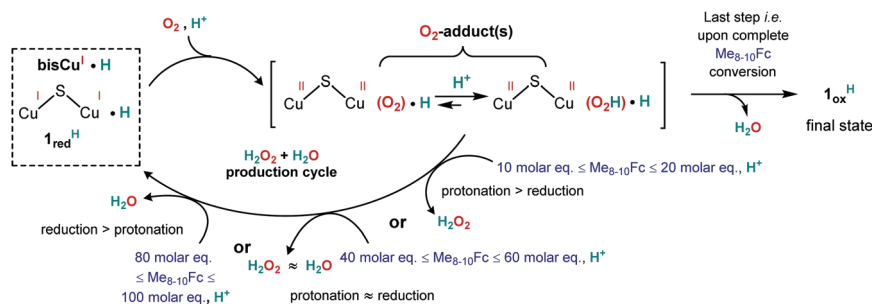
with conservation of a dinuclear delocalized MV state (absorbance in the NIR region). As expected, Me₈Fc in excess can reduce **1** to form **1_{red}**. Addition of both the electron and proton sources results in the formation of Me₈Fc⁺, the loss of the MV signature of **1** and the generation of the reduced/protonated form **1_{red}^H**. In this case, the spectrum of the final mixture can be adjusted by combining 10% of the remaining **1^H**, and 0.9 molar eq. Me₈Fc⁺ and 9.1 molar eq. Me₈Fc. **1_{red}^H** should weakly contribute to the final spectrum due to the presence of d¹⁰ Cu^I ions. In the meantime, the EPR spectra showed modifications of the hyperfine when **1** is converted into **1^H**, followed by a decrease of the signal intensity consecutive to the reduction to **1_{red}^H** (10% remaining intensity, Fig. S14, ESI[†]). An identical spectrum was obtained by adding a mixture of protons and electrons to a solution of **1**. Finally, the low-valent state was trapped by ESI-MS under similar experimental conditions (Fig. S15, ESI[†]). All these experiments provide solid evidence for a mono-electronic reduction/protonation process of **1** into **1_{red}^H** *via* **1^H**. Independently, exposure of a solution of **1_{red}^H** to air leads to full Me₈Fc consumption and the H₂O₂/H₂O ratio is in line with that reported in Table 1 (entry 1). These results clearly indicate that low-valent **1_{red}^H** is highly reactive and a key actor during catalysis.

O₂ oxidation of **1** is also considered part of the catalytic event. The corresponding **1_{ox}** form was generated by exposing a MeCN solution of **1** to air. Its crystal structure shows the presence of a double-bridged di-copper(II) unit involving the S atom from the ligand and an additional hydroxyl anion (Fig. S16, ESI[†]). **1_{ox}** has a significantly different UV-vis/NIR spectrum compared to its precursor with the loss of the NIR band (Fig. S17, ESI[†]). The extinction of the EPR signal (>90%, Fig. S18, ESI[†]) is in agreement with a strong antiferromagnetic coupling between the two metal ions leading to the S = 0 ground state. Such magnetic behaviour was already observed with a similar scaffold²⁰ or in

the case of a phenolate spacer with identical Me(*N,N*-bis(methylpyridyl))amine pendant arms.²¹ The ESI-MS spectrum of **1_{ox}** (Fig. S19, ESI[†]) shows two prominent peaks at *m/z* = 344.3 ($\Delta m/z = 0.5$) and 839.3 ($\Delta m/z = 1.0$) consistent with the solved solid-state structure. Catalytic experiments with **1_{ox}**, 10 molar eq. Me₈Fc and 400 molar eq. LutHBF₄, lead to quantitative conversion within a reaction time scale close to that of **1** (*k*_{obs} = 1.17 s⁻¹, Fig. S20 in the ESI[†]). H₂O₂ titration indicates a selectivity similar to that of **1** (88/12 for H₂O₂/H₂O). The activity of **1_{ox}** is in line with its facile protonation (to **1_{ox}^H**) and reduction (Fig. S21, ESI[†]) under anaerobic conditions. Such species could thus be part of the reactivity.

These results suggest that the H₂O₂/H₂O production cycle mainly relies on **1_{red}^H** and allow the proposition of a reaction scheme (Scheme 1). **1_{red}^H** is generated by reduction/protonation of **1** or alternatively by air oxidation/protonation/reduction of **1** *via* **1_{ox}^H** (Fig. S22, ESI[†]). O₂ activation at **1_{red}^H** followed by protonation leads to the key O₂-adduct(s) from which the selectivity can be explained by the inevitable competition between its protonation and/or reduction. Taking into account the composition of the mixture at the end of the reaction (the presence of O₂, LutHBF₄ and Me₈Fc⁺), **1_{ox}^H** is certainly the final fate of the catalyst, as observed by ESI-MS (Fig. S23, ESI[†]). This proposition is also reinforced by the ability of performing several cycles, necessarily through an oxidized species, with no loss in selectivity and efficiency. Nevertheless, **1_{ox}^H** cannot be considered as a predominantly active species during catalysis at that point, since H₂O would be the main product under any experimental condition.

To conclude, we demonstrate here that copper/sulphur assemblies such as **1** are very efficient for ORRs at room temperature with fast kinetics. By controlling the amount of Me₈₋₁₀Fc,



Scheme 1 Proposed reaction sequence for ORRs catalysed by **1_{red}^H**.

a significant and tuneable H_2O_2 vs. H_2O selectivity can be achieved. H_2O accumulation results from peroxide ligation and reduction at an active species since H_2O_2 is not reduced *in situ* in the absence of **1**. The reductive power of the reaction mixture is a factor that helps explain the selectivity. With rather “low excess” $\text{Me}_{8-10}\text{Fc}$, the two-electron reduction into H_2O_2 is favoured. When the concentration of the electron source increases, a competition between H_2O_2 release and its subsequent reduction is set up and becomes gradually predominant. Independently, a similar study with $\mathbf{1}_{\text{ox}}$ will be of great interest to compare its reactivity with a related phenolate-bridged di-copper II complex, whose ability for the ORR was reported in 2012.^{14c} The impact of the thiophenolate vs. phenolate moiety could be appreciated (at first approximations $\mathbf{1}_{\text{ox}}$ seems faster) and correlated to electronic properties. In a different light, even if H_2O_2 is quite an aggressive molecule in solution, the observation that several cycles can be performed with successive Me_8Fc injection attests to the robustness of the system. These results are encouraging for further applications in heterogeneous catalysis upon grafting air stable $\mathbf{1}_{\text{ox}}$ whether onto an inert surface in the presence of an external electron source or on electroactive materials for electrocatalysis. Finally, a global reaction sequence for the activity of **1** and its derivatives is proposed and is now under dissection with complementary kinetic experiments and characterization of the pivotal O_2 -adduct(s).

This work was supported by the Labex ARCANE and the CBH-EUR-GS (ANR-17-EURE-0003) fund *via* the CNRS, CEA and the Grenoble-Alpes University.

Conflicts of interest

There are no conflicts to declare.

Notes and references

- (a) A. Boudghene Stambouli and E. Traversa, *Renewable Sustainable Energy Rev.*, 2002, **6**, 295–304; (b) K. Mase, M. Yoneda, Y. Yamada and S. Fukuzumi, *Nat. Commun.*, 2016, **7**, 11470; (c) Y. Isaka, S. Kato, D. Hong, T. Suenobu, Y. Yamada and S. Fukuzumi, *J. Mater. Chem. A*, 2015, **3**, 12404–12412.
- W. Zhang, W. Lai and R. Cao, *Chem. Rev.*, 2017, **117**, 3717–3797.
- O. Gröger, H. A. Gasteiger and J.-P. Suchsland, *J. Electrochem. Soc.*, 2015, **162**, A2605–A2622.
- G. T. Babcock and M. Wikström, *Nature*, 1992, **356**, 301–309.
- (a) E. I. Solomon, D. E. Heppner, E. M. Johnston, J. W. Ginsbach, J. Cirera, M. Qayyum, M. T. Kieber-Emmons, C. H. Kjaergaard, R. G. Hadt and L. Tian, *Chem. Rev.*, 2014, **114**, 3659–3853; (b) E. I. Solomon, U. M. Sundaram and T. E. Machonkin, *Chem. Rev.*, 1996, **96**, 2563–2605.
- S. F. Erttmann and N. O. Gekara, *Nat. Commun.*, 2019, **10**, 3493.
- H. Sies, *Redox Biol.*, 2017, **11**, 613–619.
- R. L. Myers, *The most 100 Most Important Chemical Compounds*, Greenwood Press, London, 2007.
- J. M. Campos-Martin, G. Blanco-Brieva and J. L. G. Fierro, *Angew. Chem. Int. Ed.*, 2006, **45**, 6962–6984.
- S. Fukuzumi, Y. Yamada and K. D. Karlin, *Electrochim. Acta*, 2012, **82**, 493.
- R. Kosydar, A. Drelinkiewicz and J. P. Ganhy, *Catal. Lett.*, 2010, **139**, 105–113.
- (a) M. L. Pegis, C. F. Wise, D. J. Martin and J. M. Mayer, *Chem. Rev.*, 2018, **118**, 2340–2391; (b) C. W. Machan, *ACS Catal.*, 2020, **10**, 2640–2655; (c) P. T. Smith, Y. Kim, B. P. Benke, K. Kim and C. J. Chang, *Angew. Chem. Int. Ed.*, 2020, **59**, 4902–4907; (d) Y.-M. Zhao, G.-Q. Yu, F.-F. Wang, P.-J. Wei and J.-G. Liu, *Chem. – Eur. J.*, 2019, **25**, 3726–3739; (e) L. Wang, M. Gennari, F. G. Cantú Reinhard, J. Gutiérrez, A. Morozan, C. Philouze, S. Demeshko, V. Artero, F. Meyer, S. P. de Visser and C. Duboc, *J. Am. Chem. Soc.*, 2019, **141**, 8244–8253; (f) M. Gennari, D. Brazzolotto, J. Pécaut, M. V. Cherrier, C. J. Pollock, S. DeBeer, M. Retegan, D. A. Pantazis, F. Neese, M. Rouzières, R. Clérac and C. Duboc, *J. Am. Chem. Soc.*, 2015, **137**, 8644–8653.
- (a) M. Langerman and D. G. H. Hetterscheid, *Angew. Chem. Int. Ed.*, 2019, **58**, 12974–12978; (b) D. Das, Y.-M. Lee, K. Ohkubo, W. Nam, K. D. Karlin and S. Fukuzumi, *J. Am. Chem. Soc.*, 2013, **135**, 2825–2834; (c) M. A. Thorseth, C. S. Letko, T. B. Rauchfuss and A. A. Gewirth, *Inorg. Chem.*, 2011, **50**, 6158–6162; (d) S. Fukuzumi, H. Kotani, H. R. Lucas, K. Doi, T. Suenobu, R. L. Peterson and K. D. Karlin, *J. Am. Chem. Soc.*, 2010, **132**, 6874–6875; (e) S. Kakuda, R. L. Peterson, K. Ohkubo, K. D. Karlin and S. Fukuzumi, *J. Am. Chem. Soc.*, 2013, **135**, 6513–6522.
- (a) L. Tahsini, H. Kotani, Y.-M. Lee, J. Cho, W. Nam, K. D. Karlin and S. Fukuzumi, *Chem. – Eur. J.*, 2012, **18**, 1084–1093; (b) C. Liu, H. Lei, Z. Zhang, F. Chen and R. Cao, *Chem. Commun.*, 2017, **53**, 3189–3192; (c) S. Fukuzumi, L. Tahsini, Y.-M. Lee, K. Ohkubo, W. Nam and K. D. Karlin, *J. Am. Chem. Soc.*, 2012, **134**, 7025–7035.
- X. Engelmann, E. R. Farquhar, J. England and K. Ray, *Inorg. Chim. Acta*, 2018, **481**, 159–165.
- S. Kakuda, C. J. Rolle, K. Ohkubo, M. A. Siegler, K. D. Karlin and S. Fukuzumi, *J. Am. Chem. Soc.*, 2015, **137**, 3330–3337.
- (a) S. Gentil, D. Serre, C. Philouze, M. Holzinger, F. Thomas and A. Le Goff, *Angew. Chem. Int. Ed.*, 2016, **55**, 2517–2520; (b) M. S. Thorum, J. Yadav and A. A. Gewirth, *Angew. Chem. Int. Ed.*, 2009, **48**, 165–167; (c) C. C. L. McCrory, A. Devadoss, X. Ottenwaelder, R. D. Lowe, T. D. P. Stack and C. E. D. Chidsey, *J. Am. Chem. Soc.*, 2011, **133**, 3696–3699; (d) F.-F. Wang, Y.-M. Zhao, P.-J. Wei, Q.-L. Zhang and J.-G. Liu, *Chem. Commun.*, 2017, **53**, 1514–1517.
- S. Torelli, M. Orio, J. Pécaut, H. Jamet, L. Le Pape and S. Ménage, *Angew. Chem. Int. Ed.*, 2010, **49**, 8249–8252.
- (a) C. Matsubara, N. Kawamoto and K. Takamura, *Analyst*, 1992, **117**, 1781–1784; (b) K. Takamura, C. Matsubara and T. Matsumoto, *Anal. Sci.*, 2008, **24**, 401–404.
- C. Esmieu, M. Orio, S. Torelli, L. Le Pape, J. Pécaut, C. Lebrun and S. Menage, *Chem. Sci.*, 2014, **5**, 4774–4784.
- (a) C. Belle, C. Beguin, I. Gautier-Luneau, S. Hamman, C. Philouze, J. L. Pierre, F. Thomas and S. Torelli, *Inorg. Chem.*, 2002, **41**, 479–491; (b) S. Torelli, C. Belle, I. Gautier-Luneau, J. L. Pierre, E. Saint-Aman, J. M. Latour, L. Le Pape and D. Luneau, *Inorg. Chem.*, 2000, **39**, 3526–3536.